Zero-sequence Current Suppressing Strategy for Dual Three-phase Permanent Magnet Synchronous Machines Connected with Single Neutral Point

Zongwang Li, Yuxuan Du, Jinghua Ji, Tao Tao, and Wenxiang Zhao, *Senior Member, IEEE*

***Abstract*-Dual three-phase permanent-magnet synchronous machines (DTP-PMSM) connected with a single neutral point provide a loop for zero-sequence current (ZSC). This paper proposes a novel space vector pulse width modulation (SVPWM) strategy to suppress the ZSC. Five vectors are selected as basic voltage vectors in one switching period. The fundamental and harmonic planes and the zero-sequence plane are taken into consideration to synthesis the reference voltage vector. To suppress the ZSC, a non-zero zero-sequence voltage (ZSV) is generated to compensate the third harmonic back-EMF. Rather than triangular carrier modulation, the sawtooth carrier modulation strategy is used to generate asymmetric PWM signals. The modulation range is investigated to explore the variation of modulation range caused by considering the zero-sequence plane. With the proposed method, the ZSC can be considerably reduced. The simulated and experimental results are presented to validate the effectiveness of the proposed modulation strategy.**

***Index Terms*—Zero-sequence current, a single neutral point, dual three-phase, permanent-magnet synchronous machine, third harmonic back-EMF.**

I. INTRODUCTION

CONVENTIONAL three-phase PMSM has limits in situations that require high power rates and high fault tolerance. In recent years, the multi-phase machine has been widely concerned because it has the advantages of high fault tolerance, low torque ripple, and low per phase current without increasing the per phase voltage [1]-[4]. A typical type of multi-phase is the asymmetric six-phase machine, consisting of two groups of three-phase stator windings with phase-shifted by 30º. This dual three-phase machine has the advantages of well-developed three-phase ones [5]-[7]. However, two sets of mutually coupled stator windings induce the harmonic current. In [8], the dual three-phase induction machine was decoupled into three related subspaces by vector space decomposition (VSD). The fundamental space involves electromechanical energy conversion. The harmonic space and the zero-sequence subspace correspond to non-electromechanical energy conversion. The dual three-phase machine can be connected by either isolated neutral points or a common neutral point. Machines configured with isolated neutral points have attracted more attentions because it consists of no circulates of ZSC.

Space vector voltage pulse width modulation (SVPWM) based on the VSD for dual three-phase machine connected by isolated neutral pointes was firstly proposed in [8] to suppress the harmonics. A new PWM strategy based on 24–sector VSD was presented in [9]. Different switching sequences were analyzed by comparing the harmonic performance. Meanwhile, discontinuous and continuous modulation strategies under different voltage ranges were investigated. In order to reduce the switching loss, three PWM strategies for dual three-phase machines were presented in [10]. Ref. [11] proposed a synchronized SVPWM that includes more switching patterns, and each pattern has multiple implementations. The over-modulation occasion was considered, and the solution was proposed to guarantee the machine operation in the full modulation range.

All the SVPWM strategies mentioned above are based on the dual three-phase machines configured with isolated neutral points. SVPWM strategies for dual three-phase machines connected with a common neutral point have rarely been studied. Ref. [12] investigated the fault-tolerant performance under one open-phase fault of the dual three-phase machine configured with both isolated and a common neutral point. The results have demonstrated that machines connected with a single neutral point show superior post-fault performance than isolated neutral points. However, the typology with a single neutral point operated in healthy mode provides a loop for ZSC, which acts as the third harmonic component. The ZSC induces additional winding loss without contributing to electromechanical energy conversion. Conventional four-vector SVPWM strategies for topology with isolated neutral points induce ZSC because the zero-sequence subspace is not taken into consideration. Unlike induction

Manuscript received February 16, 2022; accepted May 10, 2022. date of publication December 25, 2022; date of current version December 18, 2022.

This work was supported in part by the National Natural Science Foundation of China under Grant 51977099. *(Corresponding author: Jinghua Ji)*

The authors are with the School of Electrical and Information Engineering, Jiangsu University, Zhenjiang 212013, China (e-mail: 2212007010@stmail.ujs.edu.cn; dyx@stmail.ujs.edu.cn; jjh@ujs.edu.cn; taotao0511@ujs.edu.cn; zwx@ujs.edu.cn).

Digital Object Identifier 10.30941/CESTEMS.2022.00058

machine, the ZSC of the DTP-PMSM is not only produced by zero-sequence voltage (ZSV) generated by modulation scheme but also produced by zero-sequence back electromotive force (EMF).

The novelty of this paper is to suppress the ZSC of the DTP-PMSM connected by a single neutral point. Three subspaces will be taken into consideration to generate the reference voltage vector. To suppress the ZSC, zero-sequence voltage (ZSV) is generated to compensate for the third harmonic back-EMF. The rest of this paper is organized as follows. In Section II, the mode of vector space decomposition is briefly introduced, and the zero-sequence circulates is analyzed. Section III presents the principle of the proposed ZSC suppression strategy and the implementation of modulation. The modulation range is analyzed. Finally, the simulated and experimental results are shown in Section IV, and Section V concludes this paper.

II. Vector Space Decomposition and ZSC Circulates

Fig. 1 shows the DTP-PMSM with a common neutral point powered by a six-phase voltage source inverter (VSI). U_{dc} is the DC bus voltage, and each phase has upper and lower bridge arms. The on and off of the power switch is controlled by the PWM signals, and only one switch of each phase is turned on simultaneously. The switching function can be defined as S=[S_a S_b S_c S_d S_e S_f]. Taking phase-a as an example, S_a=1 represents the upper-side switch is turned on, S_a=0 represents the lower-side switch is turned on. According to the principle of VSD, the voltage vector in the α-β subspace, $z1$-$z2$ subspace, and $o1$-$o2$ subspace can be expressed as (1)-(3).

$$U_{\alpha-\beta}=\frac{U_{dc}}{3}(S_a+S_b a^4+S_c a^8+S_d a^2+S_e a^5+S_f a^9) \quad (1)$$

$$U_{z1-z2}=\frac{U_{dc}}{3}(S_a+S_b a^8+S_c a^4+S_d a^5+S_e a^1+S_f a^9) \quad (2)$$

$$U_{o1-o2}=\frac{U_{dc}}{6}(S_a o+S_b o+S_c o-S_d o^3-S_e o^3-S_f o^3) \quad (3)$$

where $a=e^{j\pi/6}$, $o=e^{j\pi/4}$. The subscript of each voltage vector is written as a combination of two octal numbers, which is obtained by the binary switching function. For example: u_{45} represents the switching function S=[1 0 0 1 0 1].

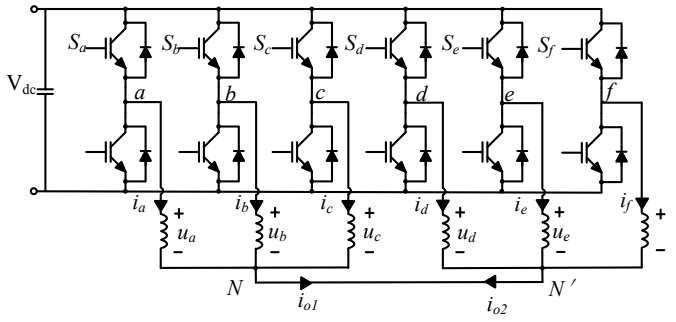

Fig. 1. DTP-PMSM with common neutral point fed by six-phase voltage source inverter.

According to the combination of different switching states of each phase, 64 space voltage vectors can be obtained, including 60 active vectors and 4 zero vectors (u_{00}, u_{07}, u_{70}, u_{77}). According to the magnitude, the active vectors the in α-β plane and $z1$-$z2$ plane can be divided into four categories: large vector U_L, medium-large vector U_{ML}, medium-small vector U_{MS} and small vector U_S. The amplitudes of them are expressed as (4).

$$\begin{cases} U_L=\dfrac{2}{3}U_{dc}\cos\dfrac{\pi}{12}=\dfrac{\sqrt{6}+\sqrt{2}}{6}U_{dc} \\ U_{ML}=\dfrac{2}{3}U_{dc}\cos\dfrac{\pi}{4}=\dfrac{\sqrt{2}}{3}U_{dc} \\ U_{MS}=\dfrac{2}{3}U_{dc}\cos\dfrac{\pi}{3}=\dfrac{1}{3}U_{dc} \\ U_S=\dfrac{2}{3}U_{dc}\dfrac{5\pi}{12}=\dfrac{\sqrt{6}-\sqrt{2}}{6}U_{dc} \end{cases} \quad (4)$$

The distribution of all the 64 vectors in the α-β plane and $z1$-$z2$ plane are illustrated in Figs. 2 and 3, respectively. The large vectors in the α-β plane correspond to the small vectors in the $z1$-$z2$ plane, while the small vectors in the α-β plane is the large vectors in the $z1$-$z2$ plane. The medium-large and medium-small vectors in the α-β plane remain the medium-large and medium-small vectors in the $z1$-$z2$ plane.

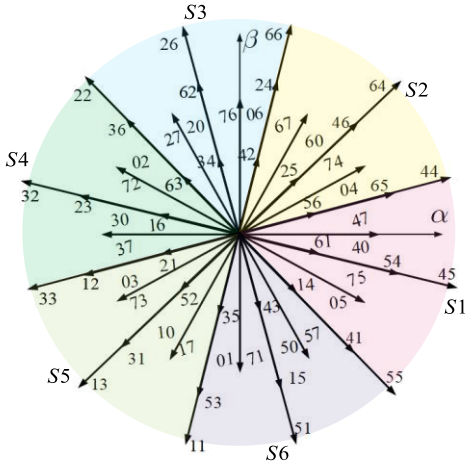

Fig. 2. Voltage vectors distribution in α-β plane.

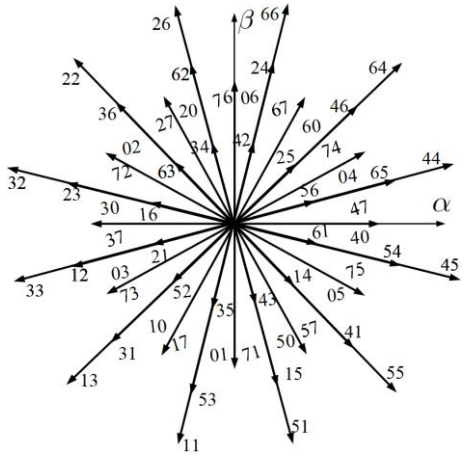

Fig. 3. Voltage vectors distribution in $z1$-$z2$ plane.

The distribution of all the 64 vectors in the $o1$-$o2$ plane is shown in Fig. 4. The vectors in $o1$-$o2$ plane can be divided into seven categories with amplitude of 0, $\pm U_{dc}/6$, $\pm U_{dc}/3$,

$\pm U_{dc}/2$. It can be seen that the distribution of 64 vectors is on a line. Therefore, the zero-sequence circuit can be seen as a one dimension system.

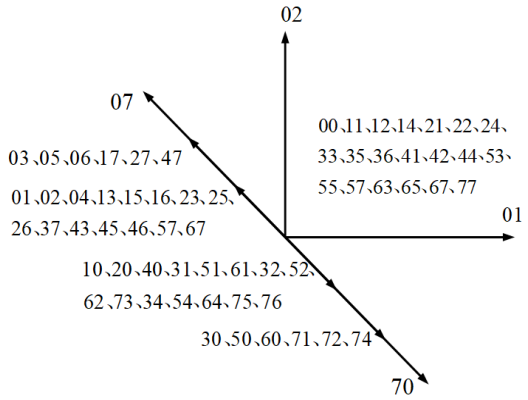

Fig. 4. Voltage vector distribution in $o1$-$o2$ plane.

It can be seen from Fig. 1 that there exists i_{o1}=-i_{o2}. When the back-EMF does not contain the third harmonic back-EMF, the equivalent circuit of zero-sequence is shown in Fig. 5(a). L_0 is the inductance of zero-sequence, and R is the resistance of phase winding. U_o is the zero-sequence voltage generated by the inverter. In this situation, the ZSC can be simply controlled by making the inverter generate zero ZSV.

When the back-EMF contains the third harmonic back-EMF, the equivalent circuit of zero-sequence is shown in Fig. 5(b). ω and θ are the electrical angular speed and electrical angle, respectively. The ZSC of DTP-PMSM is not only produced by ZSV generated by the inverter but also produced by the third harmonic back EMF. Therefore, additional compensation should be added to suppress the ZSC.

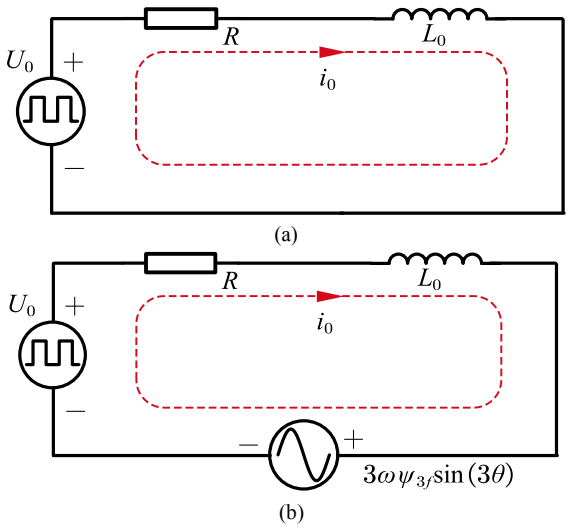

Fig. 5. Equivalent circuits of ZSC. (a) Without third harmonic back-EMF. (b) With third harmonic back-EMF.

III. Modulation With Zero-Sequence Voltage

A. *Modulation Principle*

The DTP-PMSM system can be decoupled into three subspaces, involving α-β plane, $z1$-$z2$ plane, and $o1$-$o2$ plane. The current in $z1$-$z2$ and $o1$-$o2$ planes could not contribute to the electromechanical energy conversion. Consequently, the average voltage vector in the $z1$-$z2$ and $o1$-$o2$ planes should be controlled to zero, and the voltage vector in the α-β plane should be controlled to meet the electromechanical energy conversion.

According to the above analysis, the DTP-PMSM involves three planes and can be seen as a five dimensions system. Thus, five active vectors are needed to maintain synthesis requirements in five dimensions. The proposed modulation strategy can be accomplished by the voltage-seconds equation expressed in (5). And the matrix form of (5) is presented in (6). The zero-sequence voltage constraint is illustrated in (7). When the back-EMF consists of third harmonic components, a non-zero U_o will be generated to counteract the third harmonic back-EMF.

$$U_{ref}T_s = U_1T_1 + U_2T_2 + U_3T_3 + U_4T_4 + U_5T_5 \tag{5}$$

$$\begin{bmatrix} U_\alpha \\ U_\beta \\ U_{z1} \\ U_{z2} \end{bmatrix} T_s = \begin{bmatrix} U_{\alpha1} & U_{\alpha2} & U_{\alpha3} & U_{\alpha4} & U_{\alpha5} \\ U_{\beta1} & U_{\beta2} & U_{\beta3} & U_{\beta4} & U_{\beta5} \\ U_{z_11} & U_{z_12} & U_{z_13} & U_{z_14} & U_{z_15} \\ U_{z_21} & U_{z_22} & U_{z_23} & U_{z_24} & U_{z_25} \end{bmatrix} \begin{bmatrix} T_1 \\ T_2 \\ T_3 \\ T_4 \\ T_5 \end{bmatrix} \tag{6}$$

$$U_o = U_{o1}T_1 + U_{o2}T_2 + U_{o3}T_3 + U_{o4}T_4 + U_{o5}T_5 \tag{7}$$

where U_{ref} is the reference voltage vector. T_s is the switching period. T_i (i=1, 2, 3, 4, 5) is the duration time of U_i (i=1, 2, 3, 4, 5). U_{ij} is the jth vector's projection on i axis. U_n (n=α, β, $z1$, $z2$, $o1$) are the reference voltage vectors of n axis.

The dwell time of active vectors can be obtained by (6) and (7). The rest of the time will be assigned to zero vector "u_{00}", and the duration time T_0 can be obtained by (8).

$$T_0 = T_s - (T_1 + T_2 + T_3 + T_4 + T_5) \tag{8}$$

A group of five vectors should be selected to synthesize the reference voltage vector in every switching period. The selected five vectors should guarantee the solution of T_i has a unique and positive value. There are many ways to choose such a group of five vectors. In order to obtain voltage utilization as high as possible, the vectors with magnitude as large as possible should be used to synthesize the reference voltage vector. The basic vectors used in this paper are outmost 12 vectors. As shown in Fig. 2, the α-β plane is divided into six sectors. The vectors selected in Sector 1 (S1) are 51 – 55 – 45 – 44 – 64. The vectors used in other Sectors are listed in Table Ⅰ.

TABLE Ⅰ
SELECTED VECTORS

Sector	Vectors				
1	51	55	45	44	64
2	45	44	64	66	26
3	64	66	26	22	32
4	26	22	32	33	13
5	32	33	13	11	51
6	13	11	51	55	45

B. *Implementation of Modulation*

The T_i obtained from (6) and (7) will be used to generate switching signals. Taking Sector 1 as an example, the vectors employed in Sector 1 will generate asymmetric switching signals, as shown in Fig. 6. Traditional triangular carrier is not suitable for this situation because symmetric switching signals

will generate an error with the reference vectors. A sawtooth carrier modulation strategy is employed to generate switching signals.

Fig. 6 shows the principle of sawtooth carrier modulation. The carrier amplitude is 1. Each phase has two comparison values per cycle. When the carrier value is equal to the comparison value 1 (CMP1), the switch signal changes from 0 to 1. When the carrier value is equal to the comparison value 2 (CMP2), the switch signal changes from 1 to 0. Fig. 5 shows the switching signals of the maximum five-vector SVPWM in Sector 1 when the sawtooth carrier is implemented. It can be seen that when the sawtooth carrier is used, the pulse of each phase can be placed at any position by changing the values of comparison value 1 and comparison value 2. Consequently, asymmetrical switching signals can be generated directly. Similar modulation can be extended to other Sectors.

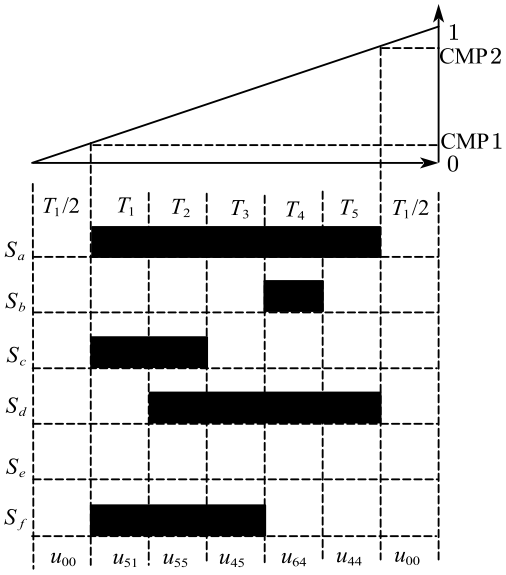

Fig. 6. Principle of the sawtooth carrier modulation.

C. *Analysis of Modulation Range*

When the modulation involves triple subspaces, the linear modulation range will be affected. Consequently, it is critical to investigate the linear modulation range of the proposed method.

Linear modulation range refers maximum fundamental plane modulation range that the synthesis magnitudes on $z1$-$z2$ and $o1$-$o2$ are zero without affecting the fundamental plane. The modulation index of the fundamental plane can be defined as (9) [14].

$$m = \frac{U_{ref}}{2/\pi\,(U_{dc})} \tag{9}$$

When the reference voltage reaches the boundary of the linear modulation range, the dwell time T_i and T_s satisfy formulation (10). Taking Sector 1 as an example, (11) can be obtained by taking T_i obtained into (10). Taking (9) into (11), the modulation index can be expressed as (12).

$$T_s = T_1 + T_2 + T_3 + T_4 + T_5 \tag{10}$$

$$(1 + \frac{\sqrt{3}}{2})\frac{u_\alpha}{u_{DC}}T_s + \frac{\sqrt{3}}{2})\frac{u_\beta}{u_{DC}}T_s = T_s \tag{11}$$

$$m = \frac{\pi}{2[\ (1+\frac{\sqrt{3}}{2})\cos\theta + (1-\frac{\sqrt{3}}{2})\sin\theta]} \tag{12}$$

where $-\pi/4 < \theta < \pi/12$.

The maximum linear modulation index can be obtained by calculating the minimum value of m. The maximum linear modulation index is 0.84. So, when the magnitude of the reference voltage is smaller than $0.535U_{dc}$, the synthesized magnitude in the harmonic plane and zero-sequence plane will not affect. Compared to the conventional four-vector SVPWM (0.9) of the DTP-PMSM configured with isolated neutral points, the proposed modulation scheme decreases the modulation index by 0.06. This is mainly caused by considering the zero-sequence plane in modulation.

IV. Simulation and Experimental Results

The simulation with the DTP-PMSM drive is performed. For a fair comparison, conventional four-vector SVPWM, as well as the proposed five-vector SVPWM, are implemented with the conventional vector control strategy. The control diagram is shown in Fig. 7. The parameters of the simulation machine model are listed in Table Ⅱ. The DC voltage is set to 200V, and the rotation speed is set to 50 r/min with a load of 100N·m. The proposed method and conventional four-vector SVPWM are simulated under the machine model without third harmonic back-EMF. The zero-sequence plane is controlled by open-loop. The simulation results of the two methods are presented in Figs. 8 and 9.

TABLE Ⅱ
PARAMETERS OF DTP-PMSM

Items	Values
PM flux ψ_f	0.96
Stator resistor	0.92Ω
d-axis inductance L_d	$15.2mH$
q-axis inductance L_q	$15.7mH$
Pole pairs	11

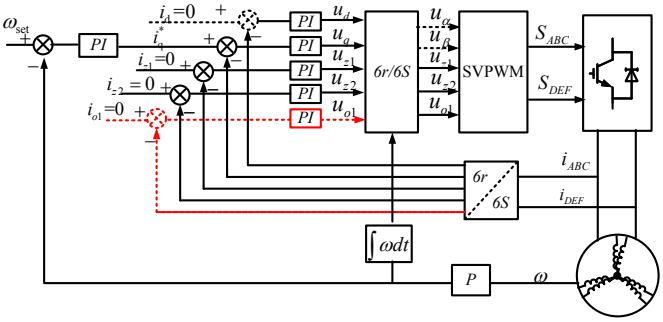

Fig. 7. Control diagram of conventional four-vector and proposed five-vector SVPWM methods.

Fig. 8 shows the simulation results of the conventional four-vector SVPWM with the topology of a common neutral point. It can be seen that conventional four-vector SVPWM induces severe phase current distortion. The maximum phase current magnitude reaches 10A, and the ZSC exceeds 20A. It

can be found that the harmonic spectrum of phase current mainly consists of third harmonic components, and the THD is 211.3%. The magnitude of the third harmonic current is more prominent than the fundamental current. This is because when the zero-sequence impedance is small, a small ZSV will lead to a large ZSC. When the back-EMF does not consist of the third harmonic back-EMF, the main ZSC is caused by ZSV generated by the inverter.

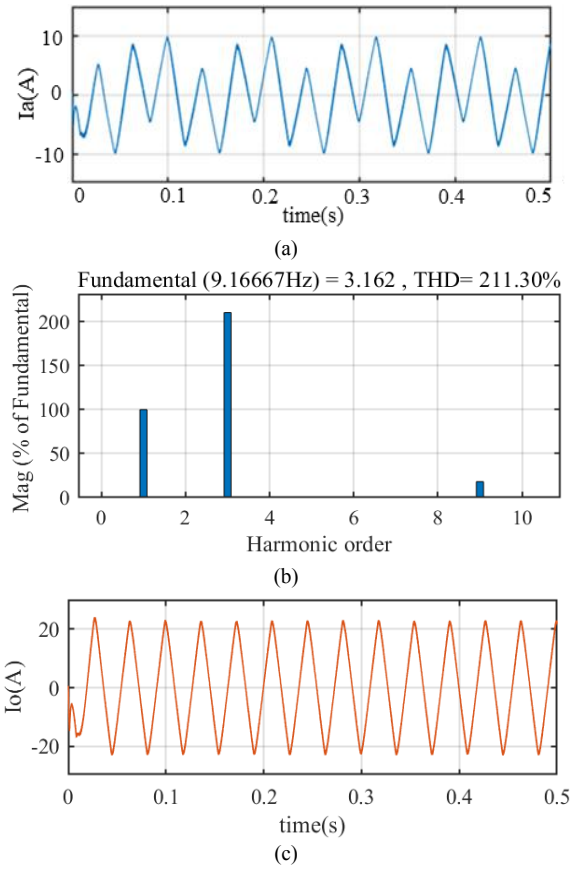

Fig. 8. Simulation results of conventional four-vector SVPWM. (a) Phase current. (b) Phase current spectrum. (c) ZSC.

Fig. 9 shows the simulation results of the proposed five-vector SVPWM. It can be found that the phase current of the proposed five-vector SVPWM is more sinusoidal than the conventional four-vector SVPWM. The maximum amplitude of phase current is reduced from 10A to 3A. Obviously, the amplitude of ZSC has been reduced from 20A to about 1A. From the harmonic spectrum of phase current, it can be concluded that the proposed modulation scheme causes lesser THD than conventional four-vector SVPWM. Consequently, the proposed five-vector SVPWM can successfully suppress the ZSC generated by the inverter.

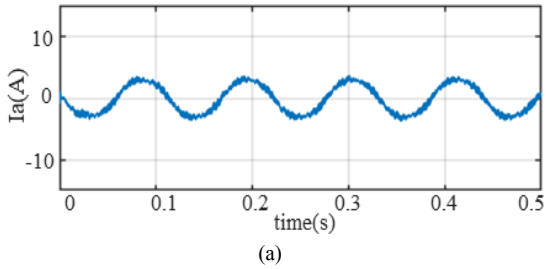

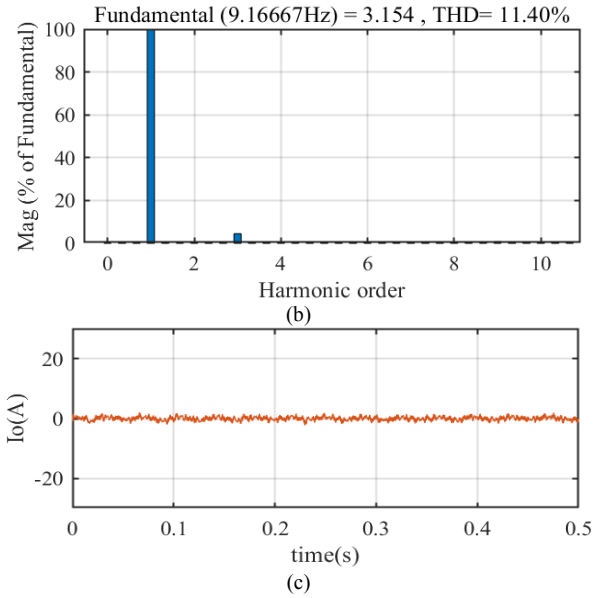

Fig. 9. Simulation results of proposed five-vector SVPWM. (a) Phase current. (b) Phase current spectrum. (c) ZSC.

The experiment was conducted on a DTP-PMSM drive system based on TMS320F28377D. The parameters of the machine are the same as the simulation model. Fig. 10 shows the experimental platform. Both the proposed and conventional methods are implemented under the condition that the DC voltage is set to 200V, and the rotation speed is set to 50r/min with the load of 100N·m. The proposed five-vector SVPWM with zero-sequence open-loop control as well as the conventional four-vector SVPWM are tested with the conventional vector control strategy, and the results are shown in Figs. 11 and 12.

The results of conventional four-vector SVPWM are presented in Fig. 11. It can be seen that the phase current of conventional four-vector has obviously been distorted. The amplitude of ZSC is 1.7A, and the THD of phase current is 29.7%. The ZSC is relatively high because the conventional method does not consider the zero-sequence plane.

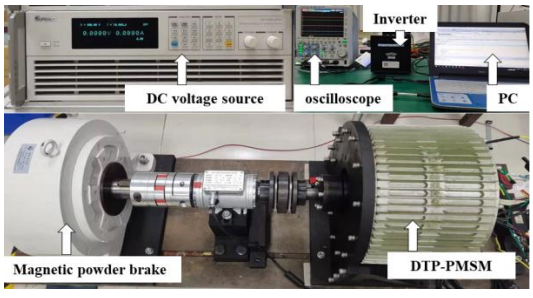

Fig. 10. Experimental platform.

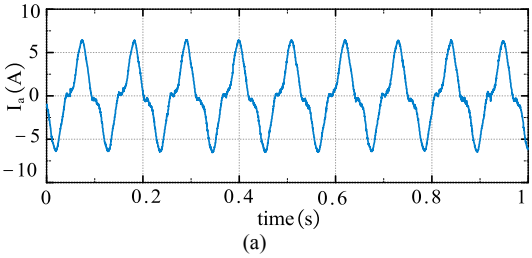

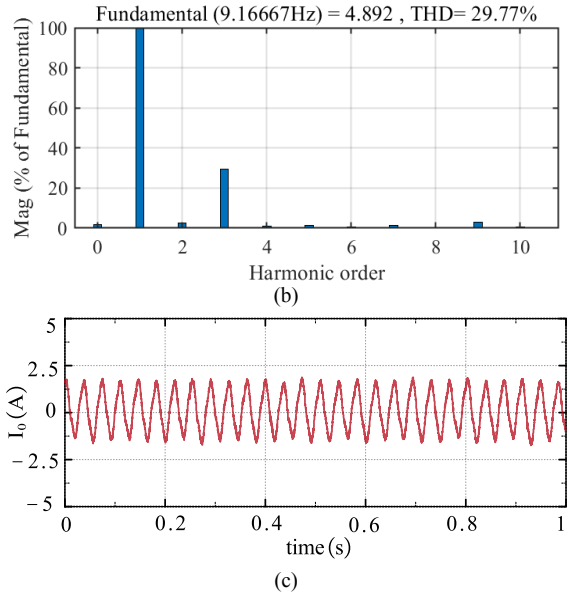

Fig. 11. Experimental results of conventional four-vector SVPWM. (a) Phase current. (b) Phase current spectrum. (c) ZSC.

The results of the proposed five-vector without zero-sequence compensation are shown in Fig. 12. As demonstrated in the simulation, the ZSV generated by modulation can be neglected in this situation. However, phase current has distorted severely compared to conventional four-vector SVPWM. The ZSC reaches 4.5A, which is larger than the conventional method. The main harmonic component is the third harmonic current, and the THD is 80.9%. This is because when the inverter does not generate ZSV, the main ZSV is generated by the third harmonic back-EMF. The third harmonic back-EMF is partially canceled by ZSV generated by the conventional four-vector SVPWM. Therefore, the ZSC of the conventional method is smaller than the proposed method without zero-sequence compensation.

In this case, additional ZSV compensation should be added to suppress ZSC. As shown in Fig. 7, a PI controller is used to generate ZSV to counteract the third harmonic back-EMF. The results are shown in Fig. 13. It can be seen that phase current

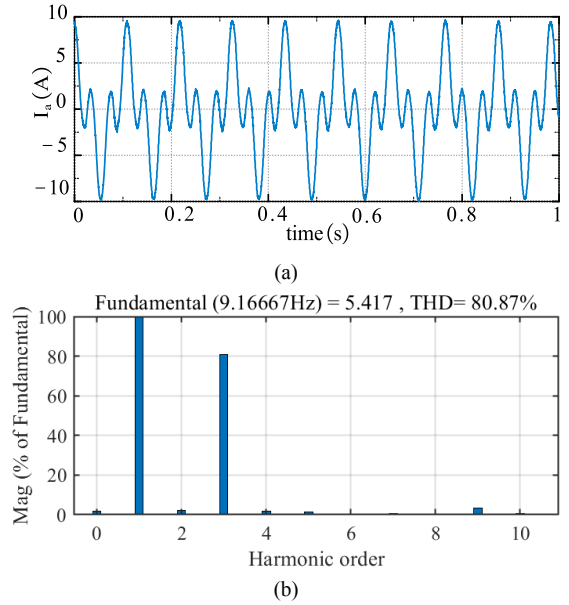

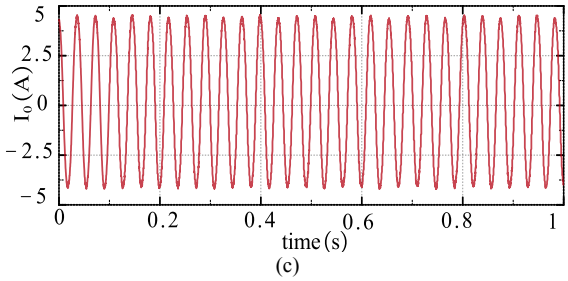

Fig. 12. Experimental results of the proposed five-vector SVPWM without zero-sequence compensation. (a) Phase current. (b) Phase current spectrum. (c) ZSC.

has been significantly improved with the ZSC compensation. The ZSC is reduced from 4.5A before compensation to 0.4A. Compared to the conventional four-vector SVPWM, the proposed five-vector SVPWM with ZSC compensation has reduced the ZSC from 1.7A to 0.4A. It can be seen from the spectrum that the THD is 8.1% which is smaller than either the conventional four-vector SVPWM or the proposed five-vector SVPWM without ZSC compensation. Consequently, the proposed modulation strategy can suppress the ZSC when the back-EMF consists of third harmonic components. That coincides with theoretical analysis.

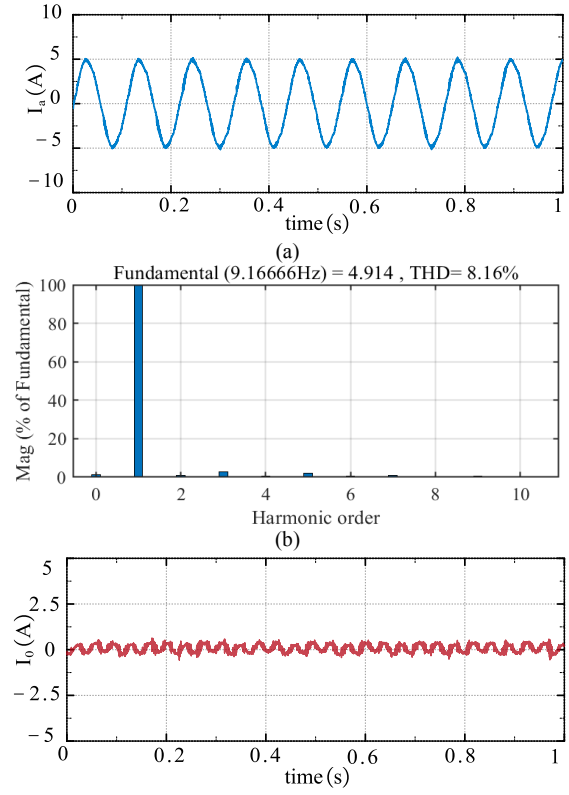

Fig. 13. Experimental results of proposed five-vector SVPWM with zero-sequence compensation. (a) Phase current. (b) Phase current spectrum. (c) ZSC.

V. Conclusion

This paper has proposed a novel five-vector SVPWM method to suppress the ZSC of the DTP-PMSM configured with a common neutral point. The proposed method uses five active vectors in one switching cycle. The fundamental and harmonic planes and zero-sequence planes have been

considered to synthesize the reference voltage. Compared with the conventional four-vector SVPWM, the proposed modulation strategy can effectively suppress the ZSC by generating reference ZSV to compensate the third harmonic back-EMF. In addition, the use of sawtooth carrier modulation mode to generate asymmetric PWM signals has avoided vector errors caused by centralization. The modulation range has been investigated to explore the variation of the modulation range caused by considering the zero-sequence plane. The simulation and experimental results have validated the effectiveness and of the proposed method.

REFERENCE

[1] E. Levi, "Multiphase electric machines for variable-speed applications," *IEEE Trans. Ind. Electron.*, vol. 55, no. 5, pp. 1893–1909, May 2008.

[2] E. Levi, F. Barrero, and M. J. Duran, "Multiphase machines and drives-Revisited," *IEEE Trans. Ind. Electron.*, vol. 63, no.1, pp. 429–432, Jan. 2016.

[3] F. Baneira, J. Doval-Gandoy, A. G. Yepes, O. Lopez, and D. Perez-Estevez, "Control strategy for multiphase drives with minimum losses in the full torque operation range under single open-phase fault," *IEEE Trans. Power Electron.*, vol. 32, no. 8, pp. 6275–6285, Aug. 2017.

[4] B. Tian, Q. T. An, J. D. Duan, D. Y. Sun, L. Sun, and D. Semenov, "Decoupled modeling and nonlinear speed control for five-phase PM motor under single-phase open fault," *IEEE Trans. Power Electron.*, vol. 32, no. 7, pp. 5473–5486, Jul. 2017.

[5] C. Zhou, G. Yang, and J. Su, "PWM strategy with minimum harmonic distortion for dual three-phase permanent-magnet synchronous motor drives operating in the over modulation region," *IEEE Trans. Power Electron.*, vol. 31, no. 2, pp. 1367–1380, Feb. 2016.

[6] J. Karttunen, S. Kallio, P. Peltoniemi, P. Silventoinen, and O. Pyrhonen, "Decoupled vector control scheme for dual three-phase permanent magnet synchronous machines," *IEEE Trans. Ind. Electron.*, vol. 61, no. 5, pp. 2185–2196, May. 2014.

[7] E. Mese, Y. Yasa, H. Akca, M. G. Aydeniz, and M. Garip, "Investigating operating modes and converter options of dual winding permanent magnet synchronous machines for hybrid electric vehicles," *IEEE Trans. Energy Convers.*, vol. 30, no. 1, pp. 285–295, Mar. 2015.

[8] Y. F. Zhao, and T. A. Lipo, "Space vector PWM control of dual three-phase induction machine using vector space decomposition," *IEEE Trans. Ind. Appl.*, vol. 31, no. 5, pp. 1100–1109, Sep./Oct. 1995.

[9] K. Marouani, L. Baghli, D. Hadiouche, A. Kheloui, and A. Rezzoug, "A new PWM strategy based on a 24-sector vector space decomposition for a six-phase VSI-fed dual stator induction motor," *IEEE Trans. Ind. Electron.*, vol. 55, no. 5, pp. 1910–1920, May. 2008.

[10] S. M. Suhel, and R. Maurya, "A new switching sequences of SVPWM for six-phase induction motor with features of reduced switching losses," *CES TEMS*, vol. 5, no. 2, pp. 100–107, Jun. 2021.

[11] L. Wu, J. Li, Y. Lu, and K. He, "Strategy of synchronized SVPWM for dual three-phase machines in full modulation range," *IEEE Trans. Power Electron.*, vol. 37, no. 3, pp. 3272–3282, Mar. 2022.

[12] H. S. Che, M. J. Duran, E. Levi, M. Jones, W. Hew, and N. A. Rahim, "Post-fault operation of an asymmetrical six-phase induction machine with single and two isolated neutral points," *IEEE Trans. Power Electron.*, vol. 29, no. 10, pp. 5406–5416, Oct. 2014.

[13] Z. Shen, D. Jiang, L. Zhu, Y. Xu, T. Zou, and Z. Liu, "A novel zero-sequence current elimination PWM scheme for an open-winding PMSM with common DC bus," *IEEE Trans. Power Electron.*, vol. 34, no. 12, pp. 12476–12490, Dec. 2019.

[14] W. Hu, H. Nian, and D. Sun, "Zero-sequence current suppression strategy with reduced switching frequency for open-end winding PMSM drives with common DC bus," *IEEE Trans. Ind. Electron.*, vol. 66, no. 10, pp. 7613–7623, Oct. 2019.

[15] H. Zhan, Z. Q. Zhu, and M. Odavic, "Analysis and suppression of zero sequence circulating current in open winding PMSM drives with common DC bus," *IEEE Trans. Ind. Appl.*, vol. 53, no. 4, pp. 3609–3620, July–Aug. 2017.

[16] W. Zhao, B. Wu, Q. Chen, and J. Zhu, "Fault-tolerant direct thrust force control for a dual inverter fed open-end winding linear vernier permanent magnet motor using improved SVPWM," *IEEE Trans. Ind. Electron.*, vol. 65, no. 9, pp. 7458–7467, Sep. 2018.

[17] A. Edpuganti, and A. K. Rathore, "New optimal pulse width modulation for single DC-link dual-inverter fed open-end stator winding induction motor drive," *IEEE Trans. Power Electron.*, vol. 30, no. 8, pp. 4386–4393, Aug. 2015.

[18] A. Cervone, M. Slunjski, E. Levi, and G. Brando, "Optimal third-harmonic current injection for asymmetrical multiphase permanent magnet synchronous machines," *IEEE Trans. Ind. Electron.*, vol. 68, no. 4, pp. 2772–2783, Apr. 2021.

[19] Z. Liu, P. Wang, W. Sun, Z. Shen, and D. Jiang, "Sawtooth carrier-based PWM methods with common-mode voltage reduction for symmetrical multiphase two-level inverters with odd phase number," *IEEE Trans. Power Electron.*, vol. 36, no. 1, pp. 1171–1183, Jan. 2021.

[20] L. Yan, Z. Q. Zhu, J. Qi, Y. Ren, and C. Gan, S. Brockway, "Suppression of major current harmonics for dual three-phase PMSMs by virtual multi three-phase systems," *IEEE Trans. Ind. Electron.*, vol. 69, no. 6, pp. 5478–5490, Jun 2022.

[21] G. Liang, W. Liao, Z. Zhang, D. Ni, S. Huang, M. Li, and Y. Wen, "An optimized pulse width modulation for dual three-phase PMSM under low carrier ratio," *IEEE Trans. Power Electron.*, vol. 37, no. 3, pp. 3062–3072, Mar. 2022.

[22] S. Liu, and C. Liu, "Direct harmonic current control scheme for dual three-phase PMSM drive system," *IEEE Trans. Power Electron.*, vol. 36, no. 10, pp. 11647–11657, Oct. 2021.

[23] B. Zheng, J. Zou, Y. Xu, X. Lang, and G. Yu, "Torque ripple suppression based on optimal harmonic current injection in dual three-phase PMSMs under magnetic saturation," *IEEE Trans. Ind. Electron.*, vol. 69, no. 6, pp. 5398–5408, Jun. 2022.

Zongwang Li received the B.Sc. degree in East China Jiaotong University, Nanchang, China, in 2020. He is currently working toward the M.Sc. degree in electrical engineering at Jiangsu University, Zhenjiang, China.

His research interests include open-end winding topology, and control of multiphase permanent magnet machines.

Yuxuan Du received the B.Sc. degree in electrical engineering from Jiangsu University, Zhenjiang, China, in 2017. He is currently working toward the Ph.D. degree in electrical engineering at Jiangsu University, Zhenjiang, China.

His research interests include open-end winding topology, control of multiphase permanent magnet machines, and design of high-performance motor driver system.

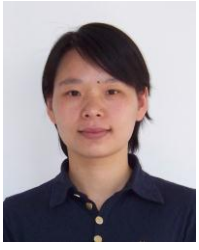

Jinghua Ji received the B.Sc., M.Sc., and Ph.D. degrees in electrical engineering from Jiangsu University, Zhenjiang, China, in 2000, 2003, and 2009, respectively.

Since 2000, she has been with the School of Electrical and Information Engineering, Jiangsu University, where

she is currently a Professor. From 2013 to 2014, she was a Visiting Scholar with the Department of Electronic and Electrical Engineering, University of Sheffield, Sheffield, U.K. Her research interests include motor design and electromagnetic field computation. She has authored or coauthored over 50 technical papers in these areas.

Tao Tao received the B.Sc. degree in electrical engineering from Nanjing Agricultural University, Nanjing, China, in 2009, and the Ph.D. degrees from Jiangsu University, Zhenjiang, China, in 2020, all in electrical engineering.

He has been with Jiangsu University since 2021, where he is currently a Lecturer in the School of Electrical Information Engineering. His research interests include control of multi-phase permanent-magnet machines.

Wenxiang Zhao (M'08–SM'14) received the B.Sc. and M.Sc. degrees from Jiangsu University, Zhenjiang, China, in 1999 and 2003, respectively, and the Ph.D. degree from Southeast University, Nanjing, China, in 2010, all in electrical engineering. He has been with Jiangsu University since 2003, where he is currently a Professor with the School of Electrical Information Engineering.

From 2008 to 2009, he was a Research Assistant with the Department of Electrical and Electronic Engineering, University of Hong Kong, Hong Kong. From 2013 to 2014, he was a Visiting Professor with the Department of Electronic and Electrical Engineering, University of Sheffield, Sheffield, U.K. His current research interests include electric machine design, modeling, fault analysis, and intelligent control. He is the author or co-author of more than 150 papers published in various IEEE TRANSACTIONS.